I&EC research
Industrial & Engineering Chemistry Research

Article

pubs.acs.org/IECR

Mixed Matrix Membranes Containing UiO-66(Hf)-$(OH)_2$ Metal−Organic Framework Nanoparticles for Efficient H_2/CO_2 Separation

Zhigang Hu, Zixi Kang,[†] Yuhong Qian, Yongwu Peng, Xuerui Wang, Chenglong Chi, and Dan Zhao*

Department of Chemical & Biomolecular Engineering, National University of Singapore, 4 Engineering Drive 4, 117585 Singapore

ABSTRACT: Mixed matrix membranes (MMMs) have received significant attention recently in the applications of gas separation for clean energy and environmental sustainability. The compatibility between dispersed functional fillers and continuous polymer matrices of MMMs is the key issue to avoid the formation of nonselective defects for better gas separation performance. Because of their easily tunable porosity, functionality, and morphology, metal−organic frameworks (MOFs) have been regarded as ideal fillers for MMMs. In this work, we present a facile modulated hydrothermal synthesis of a hafnium UiO-66-type MOF UiO-66(Hf)-$(OH)_2$ with well-defined nanoparticle size that exhibits a good compatibility with polybenzimidazole (PBI) as the polymeric matrix in the resultant MMMs. Compared to pure PBI membranes, MMMs containing MOF nanoparticles have both increased H_2 permeability and H_2/CO_2 permselectivity under optimized conditions. One of the MMMs, 10%UiO-66(Hf)-$(OH)_2$@PBI, demonstrates excellent H_2 permeability (8.12 barrers) and H_2/CO_2 permselectivity (19.37) that put it above the 2008 Robeson upper bound. Mixed-gas permeation and durability tests are also carried out to evaluate the performance of these MMMs under working conditions.

1. INTRODUCTION

The escalating increase of atmosphere CO_2 concentration caused by excessive anthropological consumption of fossil fuels has aroused worldwide concern.[1−3] Therefore, developing new and effective technologies for CO_2 capture is an urgent need.[4−6] Currently, there are three approaches to capture CO_2 from large stationary CO_2 emission points such as power plants: postcombustion CO_2 capture (CO_2/N_2 separation), precombustion CO_2 capture (H_2/CO_2 separation), and oxy-fuel combustion (O_2/N_2 separation).[7] Among these approaches, precombustion CO_2 capture is a good option because it is conducted at high CO_2 concentrations (up to 25%) and high feed pressures (20−25 bar) which are convenient for gas separation processes.[8] Because of their easy operation, facile scalability, low energy cost, and small footprint, membrane technologies have received significant attention in gas separation, especially in CO_2 capture.[9−12] However, typical polymeric membranes usually suffer from a trade-off between permeability (throughput) and selectivity (efficiency), which can be clearly depicted by the Robeson upper bounds.[13,14] Correspondingly, despite excellent thermal and chemical stability, the inorganic membranes have limitations such as weak mechanical strength and complicated fabrication procedures that make large-scale application very difficult.[15] As a result, mixed matrix membranes (MMMs) with inorganic fillers dispersed into polymeric matrices are proposed to combine the merits of both polymeric membranes and inorganic membranes.[16−18] Nevertheless, the issue of compatibility between two phases in MMMs arises, and a good adhesion of dispersed inorganic fillers toward polymeric matrices is important to avoid the formation of nonselective voids or defects.[19] It has been proven that inorganic fillers with reduced particle size such as nanoparticles and nanosheets are more stable in polymeric matrices with less agglomeration and sedimentation.[20−23] Therefore, preparing high-quality MMMs by reducing the particle size of inorganic fillers is an effective approach.

As the next generation of adsorbent materials with features such as high porosity and tailorable functionality, metal−organic frameworks (MOFs) have been widely explored recently, mainly in the areas of gas storage and separation.[24,25] Recently, there are increasing numbers of studies using MOFs as functional fillers in MMMs for gas separation.[26−28] In particular, UiO-66-type MOFs as MMM fillers have received wide attention because of their superior stability and gas separation property.[29−34] The first example of UiO-66-containing MMMs was reported by Kaliaguine and co-workers, in which UiO-66(Zr)-NH_2 MOF particles were dispersed in a synthetic 6FDA-ODA polyimide matrix with increased CO_2/CH_4 permselectivity.[30] Recently, Hill and co-workers prepared Ti-exchanged UiO-66(Zr)@PIM-1 (PIM stands for polymers of intrinsic microporosity) and found that the incorporation of MOF fillers could help to increase the gas permeability more than two-fold without a loss in the permselectivity, which was attributed to the increased CO_2 affinity toward MOF fillers.[32] As a result, even a small loading (5 wt %) of Ti-exchanged UiO-66 could improve the membrane performance dramatically to surpass the 2008 Robeson upper bound for CO_2/N_2 separation.

In our previous study, we explored the relationship of MOF filler morphology versus the gas separation performance of resultant MMMs.[35] It is found that MMMs containing MOFs with nanosheet morphology have the best gas separation performance, partially due to a high compatibility between

Special Issue: International Conference on Carbon Dioxide Utilization 2015

Received: November 30, 2015
Revised: January 16, 2016
Accepted: January 20, 2016
Published: January 29, 2016

DOI: 10.1021/acs.iecr.5b04568
Ind. Eng. Chem. Res. 2016, 55, 7933−7940

MOF fillers and polymeric matrices. In addition, we have demonstrated an effective modulated hydrothermal (MHT) approach to synthesize water-stable Zr and Hf-based UiO-66-type MOFs.[36,37] One of these MOFs, UiO-66(Hf)-$(OH)_2$, exhibits excellent H_2/CO_2 separation performance with nanoparticle morphology that serves as excellent filler in MMMs. In this work, we report such MMMs containing UiO-66(Hf)-$(OH)_2$ nanoparticles dispersed in polybenzimidazole (PBI) and their performance in precombustion CO_2 capture (H_2/CO_2 separation).

2. EXPERIMENTAL SECTION

2.1. Materials and Method. All of the reagents were obtained from commercial suppliers and used without further purification. Polybenzimidazole (PBI) was kindly provided by PBI Performance Products, Inc. Field-emission scanning electron microscopy (FE-SEM) analyses were conducted on an FEI Quanta 600 SEM instrument (20 kV) equipped with an energy dispersive spectrometer (EDS, Oxford Instruments, 80 mm^2 detector). Samples were treated via Pt sputtering before observation. Powder X-ray diffraction patterns were obtained on a Bruker D8 Advance X-ray powder diffractometer equipped with a Cu sealed tube (λ = 1.54178 Å) at a scan rate of 0.02 degree s^{-1}. Thermogravimetric analysis (TGA) was performed using a Shimadzu DTG-60AH thermal analyzer under a flowing N_2 gas (100 mL min^{-1}) with a heating rate of 10 °C min^{-1}. Dynamic light scattering (DLS) measurements were performed with a Malvern Zetasizer Nano ZS.

2.2. Synthesis of UiO-66(Hf)-$(OH)_2$. The synthesis of UiO-66(Hf)-$(OH)_2$ was carried out according to the published procedure.[36,37] Briefly, 2,5-dihydroxyterephthalic acid (1.0 g, 5.0 mmol) and $HfCl_4$ (1.7 g, 5.3 mmol) were suspended in 50 mL of water/acetic acid (30/20, v/v) mixed solvent and heated under reflux for 48 h to yield a power product. The product was soaked in anhydrous methanol for 3 days at room temperature, during which time the extract was decanted and fresh methanol was added three times. After removal of methanol by decanting, the sample was dried under vacuum at 120 °C for 24 h to yield the final product with a yield of 75% based on the total weight of ligand and metal salt.

2.3. Preparation of MMMs. Polybenzimidazole was heated at 180 °C under vacuum for at least 12 h to remove moisture and any adsorbed impurities. MMMs containing UiO-66(Hf)-$(OH)_2$ were prepared according to the published procedure.[35] Briefly, PBI (2 g) was first dissolved in *N*-methyl-2-pyrrolidone (NMP, 60 mL) by stirring at 120 °C for 48 h, followed by filtration after cooling to room temperature. UiO-66(Hf)-$(OH)_2$ of 30, 60, and 90 mg was added into dimethylformamide (DMF, 2 mL) and sonicated for 2 h to prepare 10, 20, and 30 wt % MOF-loaded MMMs, respectively. The obtained fine suspension was mixed with PBI solution (5 mL) followed by further sonication for another 2 h to give the membrane casting solution, which was casted onto a flat glass substrate and dried initially at 75 °C for 4 h and then under vacuum at 120 °C for an additional 4 h. After cooling to room temperature, the membrane was peeled off and soaked in anhydrous methanol for 3 days at room temperature, during which time the extract was decanted and fresh methanol was added three times. After removal of methanol by decanting, the membrane was further dried at 200 °C for 1 day to give the final MMMs. The thickness of MMMs (within the range from 30 to 50 μm) was measured by a micrometer caliper. The MOF loading of MMMs was calculated by the weight of MOFs divided by the total weight of MOFs plus polymers.

2.4. Single-Gas Permeation Tests. The permeability of MMMs toward single gas (H_2 and CO_2) was tested using a variable pressure constant-volume gas permeation cell technique. The setup of the gas permeation cell and testing procedures have been described previously.[35] Each test was performed after the sample was degassed to a pressure of 1−10 mTorr and the system reached thermal equilibrium after around 24 h. The operating temperature was maintained at 35 °C, and the upstream gas gauge pressure was set at 2, 3.5, and 5 bar. The gas permeability was calculated from the rate of pressure increase (dp/dt) at a steady state according to eq 1

$$P = \frac{273 \times 10^{10}}{760} \frac{VL}{AT(p_2 \cdot 76/14.7)} \left(\frac{dp}{dt}\right) \quad (1)$$

where P is the membrane gas permeability in barrer (1 barrer = 1×10^{-10} cm^3(STP) cm cm^{-2} s^{-1}·$cmHg^{-1}$); V represents the volume of the downstream reservoir (cm^3); L refers to the membrane thickness (cm); A is the effective membrane area (cm^2); T is the operating temperature (K); and p_2 indicates the upstream pressure (psia).

The ideal permselectivity of component i over component j was calculated based on eq 2

$$\alpha_{(i/j)} = \frac{P_i}{P_j} \quad (2)$$

2.5. Mixed-Gas Permeation Tests. The permeability and selectivity of MMMs toward H_2/CO_2 mixed gas (1/1, v/v) were tested using the same gas permeation cell setup described previously coupled with a Shimadzu gas chromatograph (GC-2014) equipped with HayeSep Q columns. Each test was performed after the sample was degassed to a pressure of 1−10 mTorr and the system reached thermal equilibrium after around 24 h. The operating temperature was maintained at 35 °C and the upstream gas gauge pressure was set at 3.5 and 5 bar. The mixed-gas permeability was calculated from the rate of pressure increase (dp/dt) in the downstream side at a steady state according to eq 3

$$P_i = \frac{273 \times 10^{10}}{760} \frac{y_i VL}{AT(x_i p_2 \cdot 76/14.7)} \left(\frac{dp}{dt}\right) \quad (3)$$

where P_i is the membrane mixed-gas permeability of component i in barrer (1 barrer =1 $\times$ $10^{-10}$$cm^3$(STP) cm cm^{-2} s^{-1}·$cmHg^{-1}$); x_i and y_i represent the molar fractions of component i in the upstream and downstream, respectively; V represents the volume of the downstream reservoir (cm^3); L refers to the membrane thickness (cm); A is the effective membrane area (cm^2); T is the operating temperature (K); and p_2 indicates the upstream pressure (psia).

The mixed-gas separation factor was calculated based on eq 4

$$S_{(i/j)} = \frac{y_i/y_j}{x_i/x_j} \quad (4)$$

3. RESULTS AND DISCUSSION

3.1. Preparation and Characterization of MOF Nanoparticles. UiO-66-type MOFs feature high hydrothermal and chemical stabilities that make possible their applications in industrial gas separations.[38,39] In addition, they typically exhibit

DOI: 10.1021/acs.iecr.5b04568
Ind. Eng. Chem. Res. 2016, 55, 7933−7940

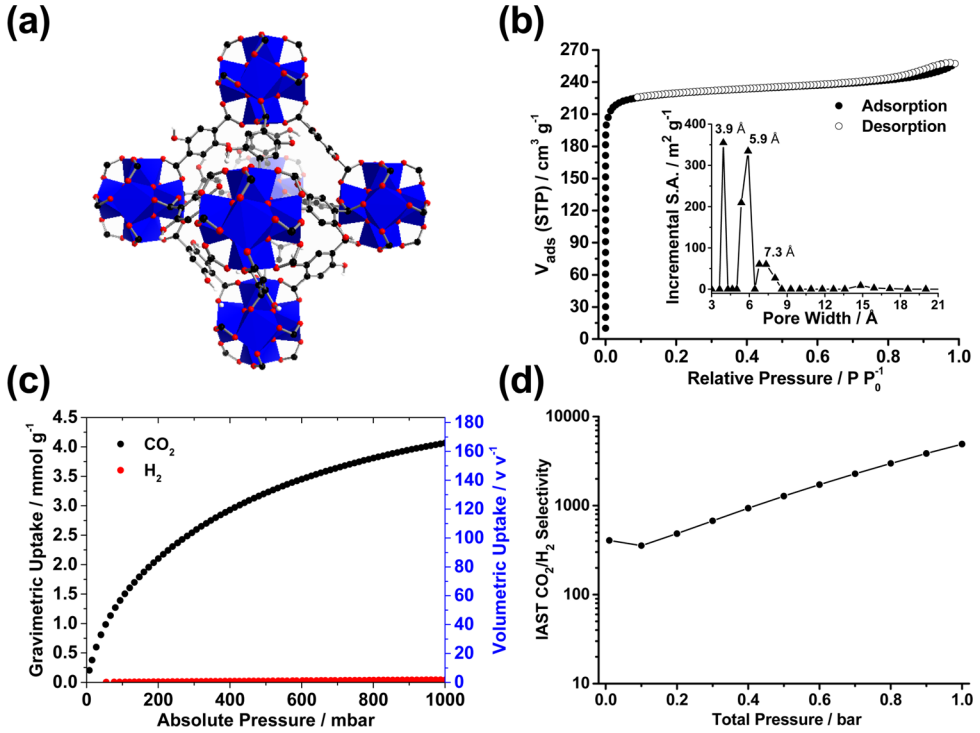

Figure 1. (a) Crystal structure of UiO-66(Hf)-$(OH)_2$ featuring the octahedral cage; (b) N_2 sorption isotherm of UiO-66(Hf)-$(OH)_2$ at 77 K (inset: pore size distribution); (c) gravimetric and volumetric CO_2 (black) and H_2 (red) uptakes of UiO-66(Hf)-$(OH)_2$ at 298 K; and (d) IAST CO_2/H_2 selectivity of UiO-66(Hf)-$(OH)_2$ calculated at 298 K assuming an equal molar mixed gas.[37] Reprinted from ref 37. Copyright 2016 American Chemical Society.

a nanoparticle morphology which is helpful in strengthening the compatibility with polymeric matrixes in MMMs.[40] In our previous study for the modulated hydrothermal (MHT) synthesis of UiO-66-type MOFs, we have synthesized UiO-66(Hf)-$(OH)_2$ with excellent hydrothermal stability.[37] This MOF has a crystal structure similar to that of UiO-66(Zr) with tetrahedral and octahedral cavities serving as gas passage channels (Figure 1a).[29] Compared to UiO-66(Zr), UiO-66(Hf)-$(OH)_2$ has a smaller Brunauer−Emmett−Teller (BET) surface area of 922 $m^2\ g^{-1}$ and reduced pore sizes at ~4 Å, possibly because of the introduction of heavier Hf cations and bulkier ligands (Figure 1b).[37] Surprisingly, it exhibits excellent gravimetric CO_2 uptake of 4.06 $mmol\ g^{-1}$ and volumetric CO_2 uptake of 167 v/v at 1 bar and 298 K (Figure 1c), which is among the highest of all the water-stable pristine MOFs without chemical decorations (e.g., amine grafting). The CO_2/H_2 selectivity of UiO-66(Hf)-$(OH)_2$ calculated based on pure component isotherms using ideal adsorption solution theory (IAST)[41] is around 4900 at 1 bar and 298 K (Figure 1d), which is also among the highest of all the MOFs reported to date.[42,43] Given these features, UiO-66(Hf)-$(OH)_2$ serves as an ideal functional filler in MMMs for precombustion H_2/CO_2 separation.

As indicated previously, fillers in MMMs with reduced particle size are preferred to prevent agglomeration and sedimentation. MOF nanoparticles are normally synthesized through fast nucleation with the addition of surfactants as stabilization agents.[44,45] Based on our previous study, MOFs synthesized through the MHT approach tend to exhibit morphology of nanoparticles instead of angular large crystals due to the heterogeneous reaction media.[34,36,37] Therefore, MHT synthesis is an effective approach to prepare MOFs as nanoparticles without referring to surfactants. The morphology of synthesized UiO-66(Hf)-$(OH)_2$ featured by quasi-spherical nanoparticles with particle size of 100−200 nm confirms the above conclusion (Figure 2a). These nanoparticles may originate from a fast and heterogeneous nucleation under

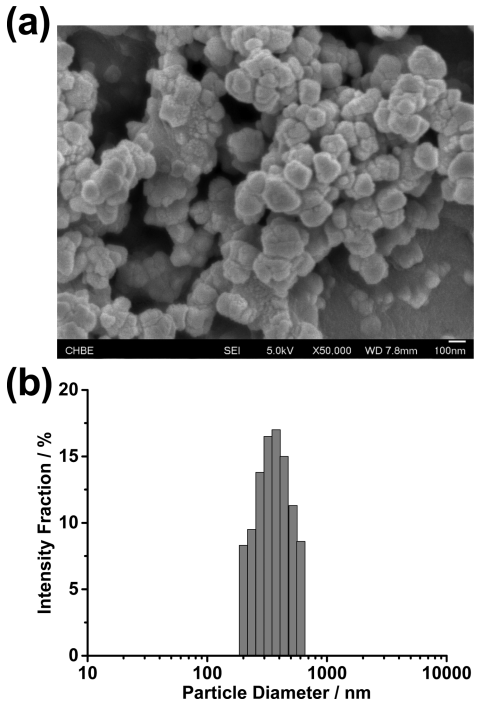

Figure 2. (a) FE-SEM image of UiO-66(Hf)-$(OH)_2$ and (b) particle size distribution of UiO-66(Hf)-$(OH)_2$ measured by dynamic light scattering (DLS).

DOI: 10.1021/acs.iecr.5b04568
Ind. Eng. Chem. Res. 2016, 55, 7933−7940

water-reflux conditions in the presence of modulators.[46] The particle size distribution measured by dynamic light scattering of UiO-66(Hf)-$(OH)_2$ dispersed in DMF solutions indicates a size distribution of 200−600 nm, which is close to the SEM results (Figure 2b). These results suggest that UiO-66(Hf)-$(OH)_2$ synthesized through the MHT approach has inherent nanoparticle morphology, which greatly facilitates its compatibility with polymeric matrices in MMMs.

3.2. Preparation and Characterization of MMMs. Polybenzimidazole is chosen as the polymeric matrix to prepare MMMs because of its excellent thermal and chemical stability as well as benchmark H_2/CO_2 separation performance among commercial polymeric membranes.[7,47] Powder X-ray diffraction (PXRD) is used to detect the crystallinity of MOF fillers. The simulated PXRD pattern of UiO-66(Hf) features two strong peaks at 7.4° and 8.5° representing (111) and (200) crystal planes, respectively (Figure 3).[29,48] A similar PXRD pattern is

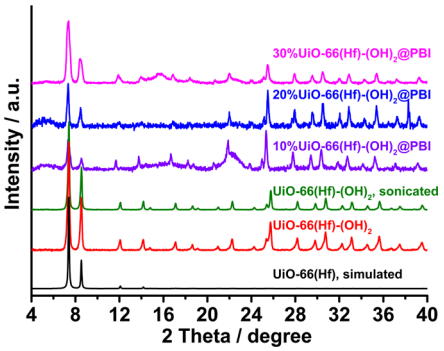

Figure 3. PXRD patterns of simulated UiO-66(Hf), as-synthesized UiO-66(Hf)-$(OH)_2$, sonicated UiO-66(Hf)-$(OH)_2$, and MMMs containing various amounts of UiO-66(Hf)-$(OH)_2$.

inherited in the MHT-synthesized UiO-66(Hf)-$(OH)_2$, confirming its isostructural feature. During the fabrication of MMMs, although UiO-66(Hf)-$(OH)_2$ is intensively sonicated, its crystallinity is still retained, indicating its excellent mechanical stability (Figure 3). The characteristic PXRD peaks belonging to UiO-66(Hf)-$(OH)_2$ can also be easily identified in MMMs, confirming the crystallinity retention of MOF nanoparticles. In our previous study, we have found specific orientation of MOF nanosheets within polymeric matrices.[35] In this case, the relative intensity of PXRD peaks remains the same between MOF nanoparticles and MMMs, suggesting an indiscriminately homogeneous distribution of MOF nanoparticles within MMMs possibly because of the quasi-spherical morphology of MOF fillers.

The even distribution of UiO-66(Hf)-$(OH)_2$ nanoparticles within PBI matrix can be directly confirmed by FE-SEM images and EDS elemental mapping shown in Figure 4. Compared to the pure PBI membrane which has a smooth texture, MMMs containing UiO-66(Hf)-$(OH)_2$ nanoparticles exhibit a plastic deformation featuring polymeric veins (Figure 4), which can be ascribed to the strong interactions between functional fillers and polymeric matrix.[49,50] The cross-sectional FE-SEM images indicate that UiO-66(Hf)-$(OH)_2$ nanoparticles have a good compatibility with PBI matrix with an even distribution ironing out possible pathways for nonselective gas permeation. In addition, the relatively even distribution of Hf element in MMMs also rules out the possibility of agglomerated MOF particles.

For power plants running under integrated gasification combined cycles (IGCC) where precombustion CO_2 capture is required, fossil fuels will be first converted into syngas (H_2/CO) followed by water−gas shift reactions to further convert H_2O and CO into H_2 and CO_2 under relatively high temperatures and pressures.[11] As a result, the operation of the succedent H_2/CO_2 separation is preferably carried out under high temperatures and pressures which require high thermal and mechanical stabilities of membrane materials. In this study, thermogravimetric analysis is applied to evaluate the thermal stability of PBI, MOF filler, and MMMs (Figure 5). Two distinct weight-loss regions can be identified in MMMs: before 150 °C for solvent loss and after 500 °C for membrane decomposition. In the case of UiO-66(Hf)-$(OH)_2$, the weight loss before 200 °C (∼18%) can be attributed to the removal of residual solvent and adsorbed water molecules, while the continuous weight loss after 200 °C suggests the degradation of organic ligands. These results suggested that MMMs containing UiO-66(Hf)-$(OH)_2$ nanoparticles can be used in conditions up to 200 °C without the risk of thermal decomposition. However, the thermal stability of MMMs is inferior to that of PBI, which is thermally stable up to 550 °C.

3.3. Single-Gas Permeation Tests. H_2 and CO_2 single-gas permeation tests are carried out for pure PBI membranes as well as MMMs to evaluate the H_2 permeability and H_2/CO_2 permselectivity. For pure PBI membranes, the permeability of both H_2 and CO_2 decreases slightly along with the increase of feed pressure, while the permeability of CO_2 decreases faster leading to increased H_2/CO_2 permselectivities under higher pressures (Table 1 and Figure 6). This is commonly encountered in glassy polymeric membranes and can be explained by the existence of strong Langmuir sorption sites in PBI membrane because it has polar functional groups with high affinity toward CO_2.[51,52]

Adding MOF nanoparticles can greatly increase the gas permeability of resultant MMMs because of the extra free volume brought by porous MOF fillers, which is helpful for gas diffusion.[28] With the increase of MOF loading, there is a significant increase in H_2 permeability from 8.21 barrers (10 wt % MOF loading) to 10.41 barrers (20 wt % MOF loading), and further to 14.94 barrers (30 wt % MOF loading) of MMMs at 2 bar. These values are 127%, 188%, and 313% higher than that of pure PBI membranes (3.62 barrers), respectively. Meanwhile, the CO_2 permeability also increases but with a larger magnitude compared to that of H_2 at higher MOF loadings, leading to reduced H_2/CO_2 permselectivity at higher MOF loadings, which is in accordance with our previous study.[35]

In general, the permeability of both H_2 and CO_2 decreases in MMMs under higher feed pressures, and CO_2 permeability drops faster, which is similar to that of pure PBI membranes. Considering the high CO_2 uptake and affinity of UiO-66(Hf)-$(OH)_2$, the strong Langmuir sorption sites for CO_2 contributed by this MOF filler could be one reason for the decreased CO_2 permeability at higher pressures. Another possible reason is the confined porous milieu introduced by MOF fillers wherein gas diffusivities decrease at higher pressures.[53] This effect will be more influential toward CO_2 over H_2 because of the larger condensability of CO_2.[54] As a result, the increase of H_2/CO_2 permselectivities at higher pressures in MOF-loaded MMMs is more obvious than in pure PBI membranes (Figure 6), leading to 10%UiO-66(Hf)-$(OH)_2$@PBI with a H_2 permeability of 8.12 barrers and H_2/CO_2 permselectivity of 19.37 at 5 bar that is above the 2008 Robeson upper bound (Figure 6). This feature

DOI: 10.1021/acs.iecr.5b04568
Ind. Eng. Chem. Res. 2016, 55, 7933−7940

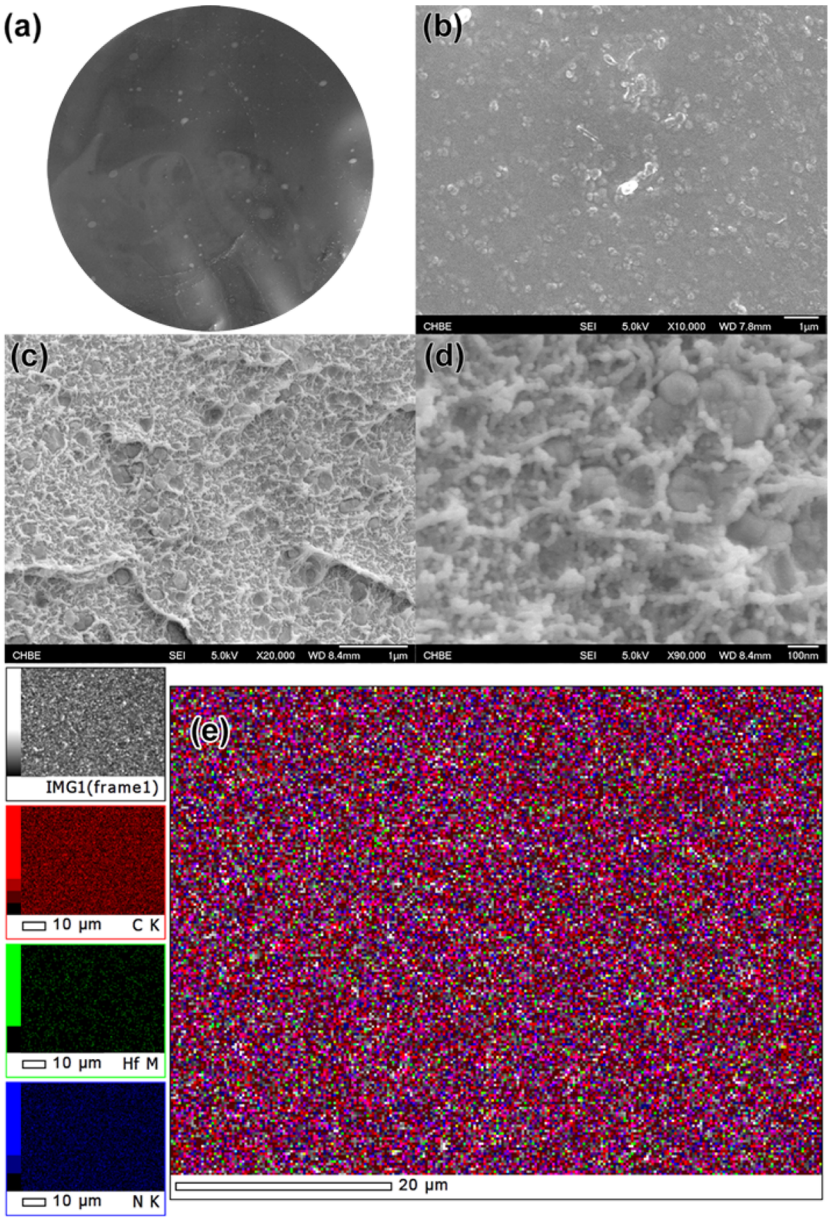

Figure 4. (a) Optical image of 10%UiO-66(Hf)-$(OH)_2$@PBI; (b) top-down FE-SEM image of 10%UiO-66(Hf)-$(OH)_2$@PBI; (c,d) cross-sectional FE-SEM images of 10%UiO-66(Hf)-$(OH)_2$@PBI; and (e) EDS elemental mapping of 10%UiO-66(Hf)-$(OH)_2$@PBI.

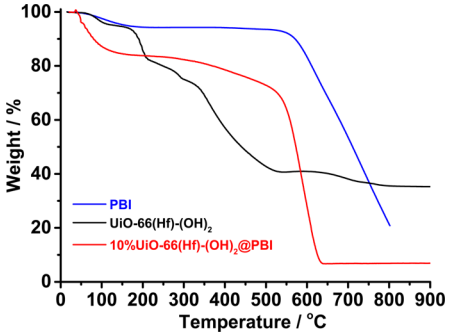

Figure 5. Thermogravimetric analysis (TGA) curves of PBI, UiO-66(Hf)-$(OH)_2$, and 10%UiO-66(Hf)-$(OH)_2$@PBI.

of increased H_2/CO_2 selectivity at higher pressures is especially attractive in precombustion CO_2 capture, which is operated at higher pressures.[8]

According to the solution-diffusion theory commonly used in polymeric membranes, the gas permeability can be expressed by the product of solubility and diffusivity. It is important to determine which one is the dominant factor. Assuming the permeability change of the MMMs in this study is controlled favorably by solubility, CO_2 permeability should increase at higher pressures because of the favorable sorption of CO_2 in MOF fillers (Figure 1c). However, this is opposite to our observation that CO_2 permeability decreases with the increase of testing pressure from 2 to 5 bar (Table 1). On the contrary, the decreased CO_2 permeability at higher pressures agrees well with the diffusion theory wherein the gas diffusivity decreases at higher pressures in confined porous media, suggesting that the gas permeability in our MMMs should be more like diffusion-controlled.

3.4. Mixed-Gas Permeation Tests. To further study the gas separation performance of MOF-loaded MMMs under practical conditions, H_2/CO_2 mixed-gas (1/1, v/v) permeation

DOI: 10.1021/acs.iecr.5b04568
Ind. Eng. Chem. Res. 2016, 55, 7933−7940

Table 1. Single-Gas (H_2 and CO_2) Permeation Properties of PBI Membranes and UiO-66(Hf)-$(OH)_2$@PBI MMMs Measured at 35 °C under Various Pressures

membrane	pressure (bar)	permeability (barrer) H_2	permeability (barrer) CO_2	H_2/CO_2 permselectivity
PBI	2	3.62 ± 0.02	0.40 ± 0.01	9.05
	3.5	3.62 ± 0.02	0.39 ± 0.02	9.28
	5	3.61 ± 0.01	0.38 ± 0.02	9.50
10%UiO-66(Hf)-$(OH)_2$@PBI	2	8.21 ± 0.05	0.69 ± 0.002	11.92
	3.5	8.13 ± 0.007	0.52 ± 0.004	15.64
	5	8.12 ± 0.01	0.42 ± 0.002	19.37
20%UiO-66(Hf)-$(OH)_2$@PBI	2	10.41 ± 0.02	1.32 ± 0.001	7.87
	3.5	10.10 ± 0.04	1.02 ± 0.002	9.88
	5	10.97 ± 0.01	0.86 ± 0.002	12.79
30%UiO-66(Hf)-$(OH)_2$@PBI	2	14.94 ± 0.06	2.41 ± 0.08	6.26
	3.5	15.44 ± 0.06	2.14 ± 0.003	7.00
	5	15.39 ± 0.06	1.94 ± 0.002	7.97

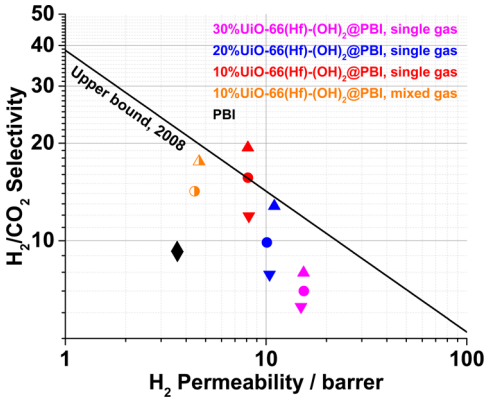

Figure 6. H_2 permeability versus H_2/CO_2 selectivity of pure PBI membranes and MMMs containing various amounts of UiO-66(Hf)-$(OH)_2$. Down-triangle, 2 bar; circle, 3.5 bar; up-triangle, 5 bar. Error bars are too small to be displayed. The 2008 Robeson upper bound for H_2/CO_2 separation is included to reflect state-of-the-art polymeric membrane performance.

tests are carried out on 10%UiO-66(Hf)-$(OH)_2$@PBI at 3.5 and 5 bar, respectively. Compared to the result of single-gas permeation tests, a 43−45% decrease of H_2 permeability is observed in mixed-gas permeation tests (Table 2 and Figure 6). This can be attributed to the CO_2-favored competitive adsorption and diffusion in MOF-loaded MMMs leading to reduced H_2 permeability.[28] However, the H_2/CO_2 separation factors have been well-retained and only slightly dropped from 15.64 (single-gas test) to 14.21 (mixed-gas test) at 3.5 bar and from 19.37 (single-gas test) to 17.55 (mixed-gas test) at 5 bar.

Table 2. Mixed-Gas (Equal Molar H_2/CO_2) Permeation Properties of 10%UiO-66(Hf)-$(OH)_2$@PBI Measured at 35 °C under Various Pressures

membrane	pressure (bar)	permeability (barrer) H_2	permeability (barrer) CO_2	H_2/CO_2 separation factor
10%UiO-66(Hf)-$(OH)_2$@PBI	3.5	4.41 ± 0.08	0.29 ± 0.005	14.21
	5	4.64 ± 0.11	0.25 ± 0.005	17.55

Membrane-based gas separation modules are expected to have long working life to reduce the operation cost. Therefore, the durability of MMMs for gas separation is another important factor to be considered. We have carried out the mixed-gas permeation test on 10%UiO-66(Hf)-$(OH)_2$@PBI for a continuous 48 h period. As can be seen from Figure 7, the membrane performance is quite stable during the test time span, indicating their strong chemical and mechanical stabilities.

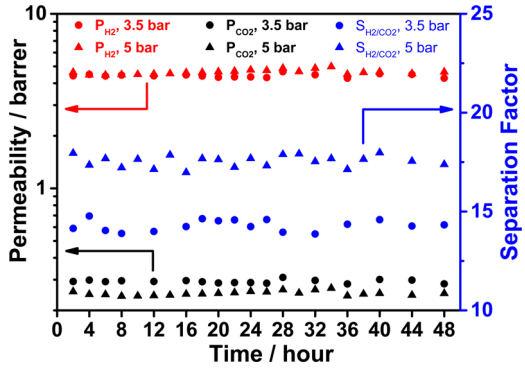

Figure 7. H_2 and CO_2 permeabilities as well as H_2/CO_2 separation factors of 10%UiO-66(Hf)-$(OH)_2$@PBI during 48 h durability tests running with an equal molar H_2/CO_2 mixed gas under various pressures (circle, 3.5 bar; up-triangle, 5 bar).

4. CONCLUSION

We have fabricated a series of MMMs using PBI as the polymeric matrix loaded with various amounts of UiO-66(Hf)-$(OH)_2$ MOF nanoparticles. Due to the strong CO_2 sorption sites and extra free volume contributed by MOF fillers, the resultant MMMs exhibit increased H_2 permeability and H_2/CO_2 selectivity compared to pure PBI membranes under optimized conditions. Among these MMMs, 10%UiO-66(Hf)-$(OH)_2$@PBI has a H_2 permeability of 8.1 barrers and H_2/CO_2 permselectivity of 19.37 at 5 bar, which puts it above the 2008 Robeson upper bound. In addition, H_2/CO_2 mixed-gas permeation tests confirmed reduced H_2 permeabilities in MOF-loaded MMMs due to the existence of CO_2-favored competitive adsorption and diffusion. The prepared MMMs demonstrate a good durability and consistent gas separation performance during a 48 h test period, which makes these membranes attractive in precombustion CO_2 capture.

AUTHOR INFORMATION

Corresponding Author

*E-mail: chezhao@nus.edu.sg.

Present Address

†Z.K.: College of Science, China University of Petroleum (East China), Qingdao, Shandong 266580, China.

Notes

The authors declare no competing financial interest.

ACKNOWLEDGMENTS

This work is supported by National University of Singapore (CENGas R-261-508-001-646) and Singapore Ministry of

DOI: 10.1021/acs.iecr.5b04568
Ind. Eng. Chem. Res. 2016, 55, 7933−7940

Education (MOE AcRF Tier 1 R-279-000-410-112, AcRF Tier 2 R-279-000-429-112).

REFERENCES

(1) Shakun, J. D.; Clark, P. U.; He, F.; Marcott, S. A.; Mix, A. C.; Liu, Z. Y.; Otto-Bliesner, B.; Schmittner, A.; Bard, E. Global warming preceded by increasing carbon dioxide concentrations during the last deglaciation. *Nature* **2012**, *484*, 49−54.

(2) Hönisch, B.; Ridgwell, A.; Schmidt, D. N.; Thomas, E.; Gibbs, S. J.; Sluijs, A.; Zeebe, R.; Kump, L.; Martindale, R. C.; Greene, S. E.; Kiessling, W.; Ries, J.; Zachos, J. C.; Royer, D. L.; Barker, S.; Marchitto, T. M.; Moyer, R.; Pelejero, C.; Ziveri, P.; Foster, G. L.; Williams, B. The geological record of ocean acidification. *Science* **2012**, *335*, 1058−1063.

(3) Myers, S. S.; Zanobetti, A.; Kloog, I.; Huybers, P.; Leakey, A. D. B.; Bloom, A. J.; Carlisle, E.; Dietterich, L. H.; Fitzgerald, G.; Hasegawa, T.; Holbrook, N. M.; Nelson, R. L.; Ottman, M. J.; Raboy, V.; Sakai, H.; Sartor, K. A.; Schwartz, J.; Seneweera, S.; Tausz, M.; Usui, Y. Increasing CO_2 threatens human nutrition. *Nature* **2014**, *510*, 139−142.

(4) Haszeldine, R. S. Carbon capture and storage: how green can black be? *Science* **2009**, *325*, 1647−1652.

(5) Markewitz, P.; Kuckshinrichs, W.; Leitner, W.; Linssen, J.; Zapp, P.; Bongartz, R.; Schreiber, A.; Müller, T. E. Worldwide innovations in the development of carbon capture technologies and the utilization of CO_2. *Energy Environ. Sci.* **2012**, *5*, 7281−7305.

(6) Boot-Handford, M. E.; Abanades, J. C.; Anthony, E. J.; Blunt, M. J.; Brandani, S.; Mac Dowell, N.; Fernández, J. R.; Ferrari, M. C.; Gross, R.; Hallett, J. P.; Haszeldine, R. S.; Heptonstall, P.; Lyngfelt, A.; Makuch, Z.; Mangano, E.; Porter, R. T. J.; Pourkashanian, M.; Rochelle, G. T.; Shah, N.; Yao, J. G.; Fennell, P. S. Carbon capture and storage update. *Energy Environ. Sci.* **2014**, *7*, 130−189.

(7) Figueroa, J. D.; Fout, T.; Plasynski, S.; McIlvried, H.; Srivastava, R. D. Advances in CO_2 capture technology - the U.S. Department of Energy's carbon sequestration program. *Int. J. Greenhouse Gas Control* **2008**, *2*, 9−20.

(8) Farrusseng, D. *Metal-Organic Frameworks: Applications from Catalysis to Gas Storage*; Wiley: Weinheim, Germany, 2011.

(9) Baker, R. W. Future directions of membrane gas separation technology. *Ind. Eng. Chem. Res.* **2002**, *41*, 1393−1411.

(10) Bernardo, P.; Drioli, E.; Golemme, G. Membrane gas separation: a review/state of the art. *Ind. Eng. Chem. Res.* **2009**, *48*, 4638−4663.

(11) Scholes, C. A.; Smith, K. H.; Kentish, S. E.; Stevens, G. W. CO_2 capture from pre-combustion processes-strategies for membrane gas separation. *Int. J. Greenhouse Gas Control* **2010**, *4*, 739−755.

(12) Shah, M.; McCarthy, M. C.; Sachdeva, S.; Lee, A. K.; Jeong, H. K. Current status of metal-organic framework membranes for gas separations: promises and challenges. *Ind. Eng. Chem. Res.* **2012**, *51*, 2179−2199.

(13) Robeson, L. M. Correlation of separation factor versus permeability for polymeric membranes. *J. Membr. Sci.* **1991**, *62*, 165−185.

(14) Robeson, L. M. The upper bound revisited. *J. Membr. Sci.* **2008**, *320*, 390−400.

(15) Pera-Titus, M. Porous inorganic membranes for CO_2 capture: present and prospects. *Chem. Rev.* **2014**, *114*, 1413−1492.

(16) Chung, T. S.; Jiang, L. Y.; Li, Y.; Kulprathipanja, S. Mixed matrix membranes (MMMs) comprising organic polymers with dispersed inorganic fillers for gas separation. *Prog. Polym. Sci.* **2007**, *32*, 483−507.

(17) Dong, G. X.; Li, H. Y.; Chen, V. Challenges and opportunities for mixed-matrix membranes for gas separation. *J. Mater. Chem. A* **2013**, *1*, 4610−4630.

(18) Rezakazemi, M.; Amooghin, A. E.; Montazer-Rahmati, M. M.; Ismail, A. F.; Matsuura, T. State-of-the-art membrane based CO_2 separation using mixed matrix membranes (MMMs): an overview on current status and future directions. *Prog. Polym. Sci.* **2014**, *39*, 817−861.

(19) Moore, T. T.; Koros, W. J. Non-ideal effects in organic-inorganic materials for gas separation membranes. *J. Mol. Struct.* **2005**, *739*, 87−98.

(20) Yang, T. X.; Xiao, Y. C.; Chung, T. S. Poly-/metal-benzimidazole nano-composite membranes for hydrogen purification. *Energy Environ. Sci.* **2011**, *4*, 4171−4180.

(21) Jeong, H. K.; Krych, W.; Ramanan, H.; Nair, S.; Marand, E.; Tsapatsis, M. Fabrication of polymer/selective-flake nanocomposite membranes and their use in gas separation. *Chem. Mater.* **2004**, *16*, 3838−3845.

(22) Varoon, K.; Zhang, X. Y.; Elyassi, B.; Brewer, D. D.; Gettel, M.; Kumar, S.; Lee, J. A.; Maheshwari, S.; Mittal, A.; Sung, C. Y.; Cococcioni, M.; Francis, L. F.; McCormick, A. V.; Mkhoyan, K. A.; Tsapatsis, M. Dispersible exfoliated zeolite nanosheets and their application as a selective membrane. *Science* **2011**, *334*, 72−75.

(23) Rodenas, T.; Luz, I.; Prieto, G.; Seoane, B.; Miro, H.; Corma, A.; Kapteijn, F.; Xamena, F. X. L. I.; Gascon, J. Metal-organic framework nanosheets in polymer composite materials for gas separation. *Nat. Mater.* **2015**, *14*, 48−55.

(24) Sumida, K.; Rogow, D. L.; Mason, J. A.; McDonald, T. M.; Bloch, E. D.; Herm, Z. R.; Bae, T. H.; Long, J. R. Carbon dioxide capture in metal-organic frameworks. *Chem. Rev.* **2012**, *112*, 724−781.

(25) Li, J. R.; Sculley, J.; Zhou, H. C. Metal-organic frameworks for separations. *Chem. Rev.* **2012**, *112*, 869−932.

(26) Jeazet, H. B. T.; Staudt, C.; Janiak, C. Metal-organic frameworks in mixed-matrix membranes for gas separation. *Dalton Trans.* **2012**, *41*, 14003−14027.

(27) Zornoza, B.; Tellez, C.; Coronas, J.; Gascon, J.; Kapteijn, F. Metal organic framework based mixed matrix membranes: an increasingly important field of research with a large application potential. *Microporous Mesoporous Mater.* **2013**, *166*, 67−78.

(28) Seoane, B.; Coronas, J.; Gascon, I.; Benavides, M. E.; Karvan, O.; Caro, J.; Kapteijn, F.; Gascon, J. Metal-organic framework based mixed matrix membranes: a solution for highly efficient CO_2 capture? *Chem. Soc. Rev.* **2015**, *44*, 2421−2454.

(29) Cavka, J. H.; Jakobsen, S.; Olsbye, U.; Guillou, N.; Lamberti, C.; Bordiga, S.; Lillerud, K. P. A new zirconium inorganic building brick forming metal organic frameworks with exceptional stability. *J. Am. Chem. Soc.* **2008**, *130*, 13850−13851.

(30) Nik, O. G.; Chen, X. Y.; Kaliaguine, S. Functionalized metal organic framework-polyimide mixed matrix membranes for CO_2/CH_4 separation. *J. Membr. Sci.* **2012**, *413*, 48−61.

(31) Venna, S. R.; Lartey, M.; Li, T.; Spore, A.; Kumar, S.; Nulwala, H. B.; Luebke, D. R.; Rosi, N. L.; Albenze, E. Fabrication of MMMs with improved gas separation properties using externally-functionalized MOF particles. *J. Mater. Chem. A* **2015**, *3*, 5014−5022.

(32) Smith, S. J. D.; Ladewig, B. P.; Hill, A. J.; Lau, C. H.; Hill, M. R. Post-synthetic Ti exchanged UiO-66 metal-organic frameworks that deliver exceptional gas permeability in mixed matrix membranes. *Sci. Rep.* **2015**, *5*, 7823.

(33) Kanehashi, S.; Chen, G. Q.; Ciddor, L.; Chaffee, A.; Kentish, S. E. The impact of water vapor on CO_2 separation performance of mixed matrix membranes. *J. Membr. Sci.* **2015**, *492*, 471−477.

(34) Hu, Z. G.; Zhao, D. *De facto* methodologies toward the synthesis and scale-up production of UiO-66-type metal-organic frameworks and membrane materials. *Dalton Trans.* **2015**, *44*, 19018−19040.

(35) Kang, X. Z.; Peng, Y. W.; Hu, Z. G.; Qian, Y. H.; Chi, C. L.; Yeo, L. Y.; Tee, L.; Zhao, D. Mixed matrix membranes comprising two-dimensional metal-organic framework nanosheets for pre-combustion CO_2 capture: a relationship study of filler morphology versus membrane performance. *J. Mater. Chem. A* **2015**, *3*, 20801−20810.

(36) Hu, Z. G.; Peng, Y. W.; Kang, Z. X.; Qian, Y. H.; Zhao, D. A modulated hydrothermal (MHT) approach for the facile synthesis of UiO-66-type MOFs. *Inorg. Chem.* **2015**, *54*, 4862−4868.

(37) Hu, Z. G.; Nalaparaju, A.; Peng, Y. W.; Jiang, J. W.; Zhao, D. Modulated hydrothermal synthesis of UiO-66(Hf)-type metal-organic frameworks for optimal carbon dioxide separation. *Inorg. Chem.* **2016**, DOI: 10.1021/acs.inorgchem.5b02312.

DOI: 10.1021/acs.iecr.5b04568
Ind. Eng. Chem. Res. 2016, 55, 7933−7940

(38) DeCoste, J. B.; Peterson, G. W.; Jasuja, H.; Glover, T. G.; Huang, Y. G.; Walton, K. S. Stability and degradation mechanisms of metal-organic frameworks containing the $Zr_6O_4(OH)_4$ secondary building unit. *J. Mater. Chem. A* **2013**, *1*, 5642−5650.
(39) Wu, H.; Yildirim, T.; Zhou, W. Exceptional mechanical stability of highly porous zirconium metal-organic framework UiO-66 and its important implications. *J. Phys. Chem. Lett.* **2013**, *4*, 925−930.
(40) Schaate, A.; Roy, P.; Godt, A.; Lippke, J.; Waltz, F.; Wiebcke, M.; Behrens, P. Modulated synthesis of Zr-based metal-organic frameworks: from nano to single crystals. *Chem. - Eur. J.* **2011**, *17*, 6643−6651.
(41) Myers, A. L.; Prausnitz, J. M. Thermodynamics of mixed-gas adsorption. *AIChE J.* **1965**, *11*, 121−127.
(42) Herm, Z. R.; Swisher, J. A.; Smit, B.; Krishna, R.; Long, J. R. Metal-organic frameworks as adsorbents for hydrogen purification and precombustion carbon dioxide capture. *J. Am. Chem. Soc.* **2011**, *133*, 5664−5667.
(43) Nugent, P.; Belmabkhout, Y.; Burd, S. D.; Cairns, A. J.; Luebke, R.; Forrest, K.; Pham, T.; Ma, S. Q.; Space, B.; Wojtas, L.; Eddaoudi, M.; Zaworotko, M. J. Porous materials with optimal adsorption thermodynamics and kinetics for CO_2 separation. *Nature* **2013**, *495*, 80−84.
(44) Flügel, E. A.; Ranft, A.; Haase, F.; Lotsch, B. V. Synthetic routes toward MOF nanomorphologies. *J. Mater. Chem.* **2012**, *22*, 10119−10133.
(45) Sindoro, M.; Yanai, N.; Jee, A. Y.; Granick, S. Colloidal-sized metal-organic frameworks: synthesis and applications. *Acc. Chem. Res.* **2014**, *47*, 459−469.
(46) Hu, Z. G.; Khurana, M.; Seah, Y. H.; Zhang, M.; Guo, Z. G.; Zhao, D. Ionized Zr-MOFs for highly efficient post-combustion CO_2 capture. *Chem. Eng. Sci.* **2015**, *124*, 61−69.
(47) Pesiri, D. R.; Jorgensen, B.; Dye, R. C. Thermal optimization of polybenzimidazole meniscus membranes for the separation of hydrogen, methane, and carbon dioxide. *J. Membr. Sci.* **2003**, *218*, 11−18.
(48) Jakobsen, S.; Gianolio, D.; Wragg, D. S.; Nilsen, M. H.; Emerich, H.; Bordiga, S.; Lamberti, C.; Olsbye, U.; Tilset, M.; Lillerud, K. P. Structural determination of a highly stable metal-organic framework with possible application to interim radioactive waste scavenging: Hf-UiO-66. *Phys. Rev. B: Condens. Matter Mater. Phys.* **2012**, *86*, 125429.
(49) Perez, E. V.; Balkus, K. J.; Ferraris, J. P.; Musselman, I. H. Mixed-matrix membranes containing MOF-5 for gas separations. *J. Membr. Sci.* **2009**, *328*, 165−173.
(50) Ordoñez, M. J. C.; Balkus, K. J.; Ferraris, J. P.; Musselman, I. H. Molecular sieving realized with ZIF-8/Matrimid® mixed-matrix membranes. *J. Membr. Sci.* **2010**, *361*, 28−37.
(51) Vieth, W. R.; Howell, J. M.; Hsieh, J. H. Dual sorption theory. *J. Membr. Sci.* **1976**, *1*, 177−220.
(52) Odani, H.; Uyeda, T. Theories of sorption and transport in polymer membrane. *Polym. J.* **1991**, *23*, 467−479.
(53) Wankat, P. C. *Separation Process Engineering*; Prentice Hall: Upper Saddle River, NJ, 2007.
(54) Itkin, A. L.; Kolesnichenko, E. G. *Microscopic Theory of Condensation in Gases and Plasma*; World Scientific: Singapore, 1997

DOI: 10.1021/acs.iecr.5b04568
Ind. Eng. Chem. Res. 2016, 55, 7933−7940